Tellus (2003), 55B, 982–992
Printed in UK. All rights reserved

TELLUS

Origin of the springtime tropospheric ozone maximum over east China at LinAn in 2001

By C. Y. CHAN[1]*, L. Y. CHAN[1], H. CUI[2], X. D. ZHENG[3], Y. G. ZHENG[2], Y. QIN[2] and Y. S. LI[1], [1]*Center of Urban Environmental Technology and Management, Department of Civil and Structural Engineering, The Hong Kong Polytechnic University, Hung Hom, Hong Kong, China;* [2]*Department of Atmospheric Sciences, School of Physics, Peking University, Beijing 100871, China;* [3]*Chinese Academic of Meteorological Sciences, Beijing, 10081, China*

(Manuscript received 3 June 2002; in final form 4 April 2003)

ABSTRACT

Tropospheric ozone (O_3) profiles over the east China coast at LinAn (30.30°N, 119.75°E) were measured by electrochemical concentration cell ozonesondes in the spring of 2001. The measurement revealed that extremely high O_3 with mixing ratios up to 1200 ppbv sometimes penetrated deeply into 8.5–16 km above sea level as a result of lowering of the tropopause across the East Asia strong subtropical jet stream. In addition, high O_3 in the 75–150 ppbv range penetrated into the upper and middle troposphere following the extreme O_3 regimes and caused an overall high O_3 mixing ratio in these regions. The occurrence of the high O_3 regimes followed the propagation of dry air with low relative humidity and high potential vorticity suggesting that the O_3 is of stratospheric origin. High O_3 episodes with O_3 mixing ratios in the 75–100 ppbv range were observed in the lower troposphere and especially in the boundary layer. Trajectory analysis suggested that the O_3-rich air masses had passed through the industrialized and urbanized zones of the Pearl River Delta region of south China, northeast China coast and Yangtze River Delta region of east China. The O_3 is probably of anthropogenic origin resulting from photochemical formation from pollutants emitted from these regions. Our analysis thus revealed that over the east China coast at LinAn, stratospheric O_3 is still the predominant source of O_3 in the middle and upper troposphere, while anthropogenic sources caused a high O_3 pollution episode in the boundary layer.

1. Introduction

There have been limited studies of tropospheric O_3 over the vast landmass of mainland China and Asia despite the fact that there has been a continuous growth in air pollutant emissions as a result of rapid urban expansion and industrial and agricultural development in the region. Pollutant emissions and export from Asia, especially China, are anticipated to impact on the air quality, chemical evolution of the atmosphere and climate change on a regional and continental scale. Photochemical O_3 pollution in major urban and industrial centers of China was reported in the early 1980s by Tang et al. (1995) and more recently by Chan and Chan (2000). Luo et al. (2000) have reported a non-urban O_3 air pollution episode over eastern China. Wang et al. (2001) have recently reported their measurements of high levels of air pollutants on the east China coast over LinAn. The effect of long-range air pollutants transport from mainland Asia on surface O_3 on the East Asia coast has been reported by Akimoto et al. (1996), Newell et al. (1997), Carmichael et al. (1998) and Chan et al. (1998b). Chan and Chan (2000) have reported the impact of long-range air pollutants on surface O_3 episodes in the region of Hong Kong in south China. Jacob et al. (1999), Jaffe et al. (1999) and Yienger et al. (2000) have reported the export of air pollutants from Asia and their

*Corresponding author.
e-mail: cececychan@polyu.edu.hk

effects on background tropospheric O_3 and surface O_3 air quality in North America. Chan et al. (2001) reported the large-scale enhancement of tropospheric O_3 and subsequent surface temperature change over tropical Southeast (SE) Asia and subtropical south China as the results of the 1997 Indonesian forest fires.

Measurements of tropospheric O_3 over many parts of the world, including East Asia and the western Pacific in Japan, Taiwan and Hong Kong, show a maximum concentration in spring (e.g. Logan, 1985; Oltmans and Levy, 1992; Harris et al., 1998; Chan et al., 1998b; Langford, 1999). In the climatologically distributed tropospheric O_3 map derived from satellite data (Fishman and Brackett, 1997), tropospheric O_3 over China and East Asia shows a springtime maximum. The springtime O_3 maximum over Japan is traditionally explained by intrusion of stratospheric O_3 into the troposphere (Muramatsu et al., 1984; Wakamatsu et al., 1989; Murao et al., 1990; Austin and Midgley, 1994; Tsutumi et al., 1994; Sunwoo et al., 1994). Kajii et al. (1998) and Pochanart et al. (1999), however, reported recently that the observed spring O_3 maximum at surface stations is caused by photochemical O_3 formation involving O_3 precursors rather than intrusion of stratospheric O_3. Carmichael et al. (1998) showed with model results that the near-surface O_3 levels in the springtime over East Asia are strongly influenced by continental outflow of precursors and the strong downward transport of O_3-rich air from the upper troposphere.

Chan et al. (1998a and 1998b) reported with surface O_3 measurements and ozonesonde data that surface O_3 in Hong Kong has an autumn maximum and summer minimum. They attributed the seasonal O_3 variation to the transport patterns associated with East Asia monsoon winds. Chan et al. (2002b) showed, with an O_3–CO relationship, that photochemical productions of O_3 from pollutants emitted from mainland Asia and the eastern Asia coast are the causes of the O_3 peak in spring in the subtropical south China region. In a model study of summertime tropospheric O_3 over China, Ma et al. (2002) found that the surface O_3 over China is controlled by photochemistry in eastern China and transport processes in western China. Zhang et al. (2002) stated, with evidence from numerical model results, that the wintertime boundary layer O_3 in East Asia is dominated by photochemistry. Chan et al. (2000; 2002a) showed that part of the O_3 maximum in the lower free troposphere over Hong Kong is a result of the strong O_3 enhancements related to the O_3 build-up caused by biomass burning emissions in SE Asia.

Understanding the mechanisms leading to the formation of the spring O_3 maximum would help us determine the continuing changes of air quality, atmospheric composition and climate caused by human activities (Monk, 2001). In this paper we report tropospheric O_3 measurements over east China at LinAn (30.30°N, 119.75°E) during the spring of 2001. The focus is on studying the possible influences of stratospheric O_3 and anthropogenic O_3 in relatively unexplored mainland China.

2. Experiment

The vertical profiles of O_3, relative humidity (RH), temperature and wind were measured by a balloon-borne electrochemical concentration cell ozonesonde (model 6A) and radiosonde (RS80-15GE) from Vaisala operated by a Vaisala DigiCora MW 15 receiving system. The ozonesonde preparation and calibration procedures, quality control and assurance procedures were similar to those described by Chan et al. (1998b). The O_3 data measured by ozonesonde have precisions from ±3 to ±12% in the troposphere. The corresponding accuracies for individual ozonesonde soundings are ±6% near the ground and 7–17% in the high troposphere, where O_3 mixing ratios may be low (Komhyr et al., 1995). The experiment site is primarily a rural one at 134m ASL. The launch was performed at 5:00–6:00 UT (13:00–14:00 LST). There were a total of 28 launches from 3 March to 13 April 2001, with a trial launch on 21 February. The O_3 profiles were available every day from 3 to 13 March. After that there was at least a profile available every other day until 13 April with the exception of 4–7 April, during which time only two profiles were available.

3. Results and discussion

3.1. Vertical ozone distribution in the middle and upper troposphere

Figure 1 shows the vertical distribution of the O_3 mixing ratio from 6.0 to 16.0 km ASL from 3 March to 13 April. In this time–height color contour plot, the O_3 mixing ratio was averaged at 250 m intervals. Also shown is the vertical distribution of the two

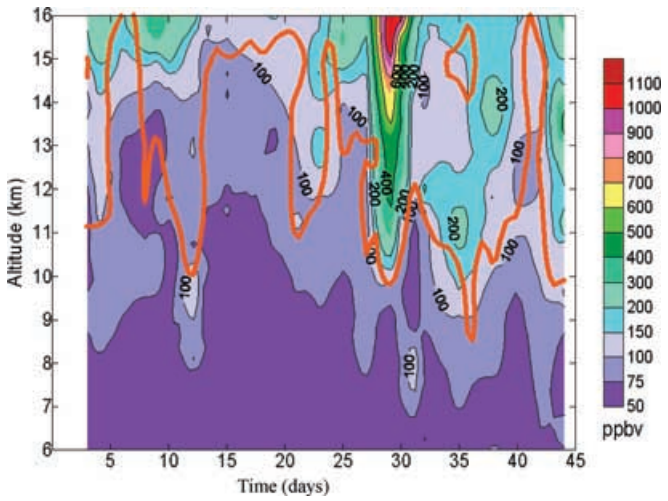

Fig. 1. Time–height contour plot of ozone mixing ratios (ppbv) between 6 and 16 km ASL from 3 March to 13 April. The thick line is the 2 PV unit surface. The time labels 5, 10, 15, 25, 30, 35, 40 and 45 correspond to 3, 5, 10, 15, 25 and 30 March and 4, 9 and 14 April, respectively.

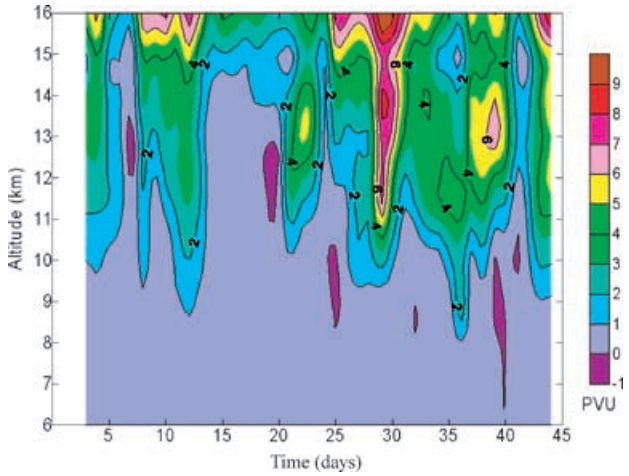

Fig. 2. Time–height contour plot of the potential vorticity (PVU, 1 PVU = 10^{-6} s^{-1} m^2 kg^{-1}) between 6 and 16 km ASL from March 3 to April 13.

potential vorticity (PV) units, which is often considered as the dynamical definition of the tropopause height at the mid-latitude. This tropopause height definition is adopted, as LinAn is located at the edge of the subtropics close to the mid-latitude. The vertical distribution of PV is shown in Fig. 2. The PV was calculated from NCEP reanalysis data. The tropopause height varied substantially from around 8.5 to 16 km. Ozone shows rather high mixing ratios and a prominent vertical variation at altitudes from 8 to 16 km. The O_3 mixing ratio varied substantially from a minimum of 50–70 ppbv at the lower region to a maximum in the 1200 ppbv range at the upper region. The most striking features in Figs. 1 and 2 are tongues of elevated O_3 mixing ratio together with elevated PV frequently extending deeply from high altitudes into altitudes from around 8.5 to 11 km. At the beginning (3–13 March), high O_3 with a mixing ratio of 100–400 ppbv extended to 10–16 km ASL. From the middle to the end of the experiment period (25 March to 9 April) extremely high

O_3 with mixing ratios in the range from 100 to over 1100 ppbv penetrated from 16 to 10.0 km ASL. At the end of the experiment period (starting from April 11) a similar elevated O_3 mixing ratio tongue reappeared. The PV values in these O_3 tongues were particularly high. For instance, at altitudes from 12.0 to 14.0 km from 20 March to 7 April, PV values greater than 5 were found at the center of the elevated O_3 mixing ratio tongues.

In addition to the high O_3 tongues, high O_3 mixing ratios of 75–150 ppbv were found in the middle and upper troposphere. Also, there was an extension of the high PV surface (1–1.5 PV units) into the upper troposphere. Noticeably, the propagation of high O_3 mixing ratios in these atmospheric regions followed that of the tropopause height. In fact, the occurrence of the two high ozone regimes (10–13 March and from March 30 to April 1), which centered at 9.5 and 7.9 km ASL, respectively, coincided or followed the elevated O_3 and tropopause tongues. Figure 3 shows the vertical distribution of relative humidity measured by the radiosondes. In general, low relative humidity was found at altitudes above 11 km. Extremely low relative humidity values were found at the regimes where enhanced O_3 mixing ratio and PV was found. However, in the periods 10–13 March and from March 29 to April 1, dry streamers penetrated down to the middle and lower troposphere at 9 and 6 km, respectively, where high O_3 values were also found. At 6–9 km altitude the relative humidity was usually in the 30–80% range.

3.2. Intrusion of stratospheric ozone in the middle and upper troposphere

The frequent occurrence of elevated O_3 tongues at high altitudes is due to a lowering of the tropopause, as indicated by the 2 PV unit surface. The air measured by ozonesonde at these altitudes is in fact stratospheric air. The simultaneous low relative humidity and high O_3 mixing ratios observed at the middle and upper troposphere over LinAn may suggest that the O_3 was of stratospheric origin. Stratospheric air is rich in O_3 and deficient in water vapor compared to tropospheric air. Ozone and water content are often considered as passive tracers of stratospheric air. In fact, O_3 and water content together with PV are usually considered conserved variables linking dynamically to the flow of stratospheric air into the troposphere in the stratosphere/troposphere O_3 exchange events (Appenzeller and Davies, 1992).

In East Asia over Japan, the exchange of stratospheric O_3 into the troposphere is often linked to the meteorological phenomenon associated with the East Asia jet stream (Muramatsu et al., 1984; Wakamatsu et al., 1989; Murao et al., 1990; Tsutumi et al., 1995). These phenomena include tropopause folds, cut-off lows and streamers along jet streams. The East Asia jet over the East Asia coast, including eastern China, is the largest jet stream in the world in spring (Ding, 1994). It comprises of a PFJ and a subtropical jet (STJ), and is linked to the presence of a semi-permanent pressure trough over the Asia continent and a large

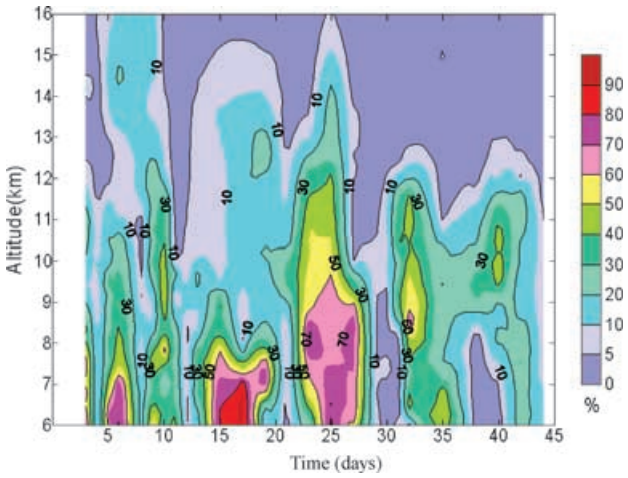

Fig. 3. Time–height contour plot of the relative humidity (%) between 6 and 16 km ASL from 3 March to 13 April.

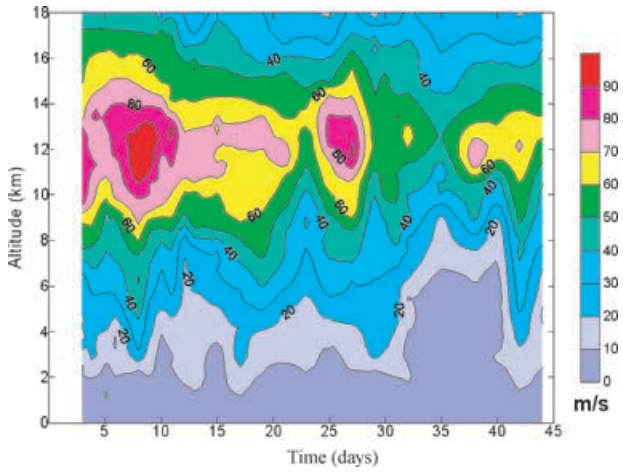

Fig. 4. Time–height plot of the wind speed (m s^{-1}) between 6 and 18 km ASL from 3 March to 13 April.

temperature contrast at the East Asia coast. Such large-scale perturbations in the flow penetrate into the westerly winds in the stratosphere and affect the distribution of O_3 available for transfer into the troposphere during spring (Austin and Midgley, 1994). Figure 4 shows the time–height cross-section of wind speed over LinAn measured simultaneously with the O_3 profiles. During the experiment period, a generally westerly wind was prevalent above the boundary layer and the wind speed was very high. The wind reached its full strength from 8–16 km with local peaks at around 10.5–13.5 km. The wind speed in this region was usually >40 m s^{-1}. The maximum reached >90 m s^{-1} on 8 March 80 m s^{-1} on 26 March and 70 m s^{-1} on 7 April. The high wind speed is associated with the STJ.

Figure 5 shows the cross-section of PV, potential temperature and wind speed along latitude across LinAn on 11 and 31 March, when a high O_3 mixing ratio was found in the upper troposphere over LinAn. Note that the O_3 enhancement regimes, especially at 9.5 km on 11 March, were within the jet stream and there were strong variations in wind speed in the vertical direction. Such strong variations in wind speed are believed to be associated with the strong wind shear within the jet stream and the nearby neighborhoods. The strong wind shear is expected to cause strong mixing in these regimes and thus transport of stratospheric O_3 in the upper and middle troposphere. In fact, the influence of the PFJ on intrusion of stratospheric O_3 into the troposphere over Japan has been confirmed by Japanese colleagues. The influence of the STJ has been noted by Tsutumi et al. (1995) and Langford (1999) through lidar O_3 measurements at the exit of the subtropical jet stream over Colorado recently. The mechanism leading to the stratospheric–tropospheric O_3 exchange over LinAn deserves detailed examination.

Austin and Midgley (1994) analyzed the ozonesonde data from Japan. The analysis showed that the stratosphere–troposphere O_3 exchange in spring is most effective over northern Japan but has little influence in the southern ozonesonde station at Kagoshima (32°N, 130°E). In our study, however, we found that such stratosphere–troposphere exchange of O_3 does contribute significantly to the O_3 in the troposphere over the middle latitudes of the east China coast at LinAn. Wakamatsu et al. (1989) reported that the stratospheric intrusion of O_3 into the troposphere may reach the lower altitudes of the troposphere and the boundary layer. However, at LinAn during the experiment period in 2001, we did not see such downward transport of O_3 into the lower troposphere. Our observational findings contrast to the recent model results from Miyazaki et al. (2003). The researchers found that the diurnal-average column-integrated rate of O_3 production in spring over East Asia is larger than the Northern Hemispheric average and local stratospheric flux at Northern Hemisphere midlatitudes by a factor of 3–20. They stressed that photochemistry controls the upper tropospheric O_3 abundance in spring.

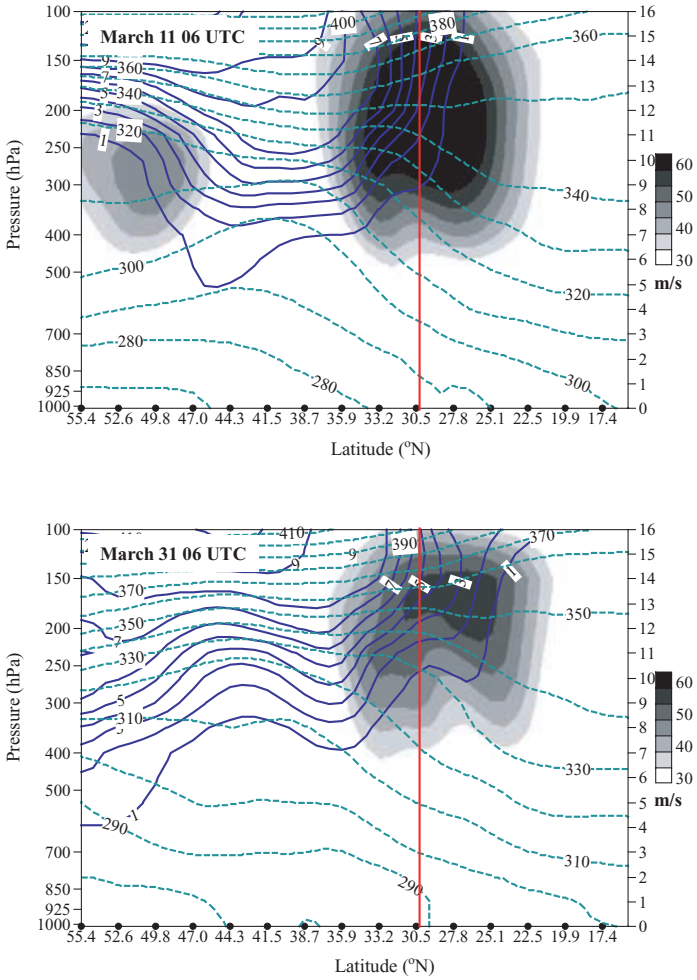

Fig. 5. The transverse vertical cross-section of wind speed (m s^{-1}) (shaded) superimposed on PV (thick blue line) and potential temperature (K) (solid green line) in a N–S direction along the axis at LinAn on 11 and 31 March at 06 UTC.

3.3. Ozone distribution in the lower troposphere and boundary layer

Figure 6 shows the vertical O_3 mixing ratio distribution below 8.0 km. Ozone shows a fairly high mixing ratio with in the range from 50 to over 100 ppbv in the lower free troposphere above 2.0 km, with exceptions from 3 to 13 March and from 25 March to 1 April, during which a low O_3 mixing ratio (<70 ppbv) extended from 7.5 km down to the surface. Noticeably, we observed isolated elevated O_3 zones with mixing ratios in the 70–100 ppbv range between 13 and 26 March and from 2 to 13 April. Ozone in the boundary layer shows comparatively greater variations. The most dominant O_3 feature in this atmospheric region is the elevated mixing ratio episodes occurring from 12 to 15 March, on March 24 and from 1 to 9 March. The O_3 mixing ratio in these periods reached a maximum of 70–100 ppbv.

Figure 7 shows the vertical profiles of O_3, relative humidity, wind speed and direction, and temperature below 8.0 km on 21 March and 7 April, corresponding to the isolated high O_3 mixing ratio zones in the lower free troposphere in Fig. 5. On 7 April, an O_3 peak with O_3 mixing ratio >100 ppbv occurred at 5.8 km above ground and a high O_3 mixing ratio region (>75 ppbv)

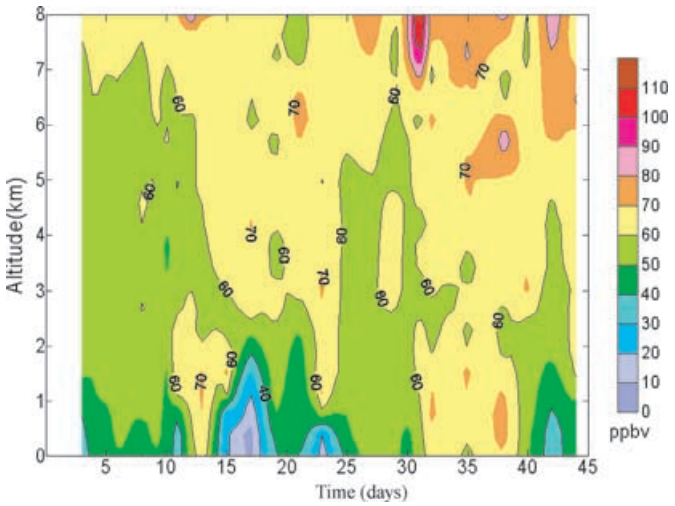

Fig. 6. Time–height contour plot of ozone mixing ratios (ppbv) below 8 km ASL from 3 March to 13 April.

at 6.8–8.0 km. The O_3 peak was accompanied by a westerly wind and the high concentration region by a general northwest wind. Noticeably, the relative humidity in the O_3 peak and the high O_3 region had extremely low values. On 21 March, a high O_3 mixing ratio in the 60–75 ppbv range extended from around 3.0 km to 7.0 km above ground. The high O_3 regime was separated from the O_3 in the boundary layer below by a strong temperature inversion below. The O_3 was also accompanied by a general west–northwest wind and extreme low relative humidity. The low relative humidity may suggest that the O_3 was a result of transport of the O_3-rich air from the middle and upper troposphere.

Figure 7 also shows the respective profiles on 15 and 23 March and 1, 4 and 7 April corresponding to the O_3 enhancement periods in the boundary layer. We noted that the elevated O_3 mixing ratio at the boundary layer on these days was accompanied by strong temperature inversions at the top of the boundary layer. On 15 March and 7 April the high O_3 was accompanied by high relative humidity values greater than 80%. On 23 March and 1 and 4 April the relative humidity values were lower, in the range 50–60%. Since the high PV region indicating stratospheric air in Fig. 3 does not penetrate below 8.0 km, direct stratospheric O_3 intrusion into the lower troposphere and the boundary layer does not seem to be the cause of the high O_3 in these atmospheric regimes over LinAn. We thus explored the source region of the elevated O_3 by isentropic back air trajectory.

3.4. Transport pattern and source region of boundary layer ozone

Figure 8 shows the 5-d back air trajectories ending at 850 hPa ($\sim$1.4 km) altitude over LinAn at 00 UTC on 15 and 23 March and 1, 4 and 7 April, corresponding to the O_3 enhancement region in Fig. 6. Also shown are the vertical motions of the trajectories. The markings in this figure show the position of the air mass every 6 h. The trajectories were calculated by the model developed by Yamazaki et al. (1989) and Murayama et al. (1998) using the NCEP reanalysis data as input. The data had a time resolution of 12 h, horizontal resolution of 1° and vertical resolution of 27 layers. The trajectory model determined the transport paths of hypothetical air parcels started at any selected isobar surface every 6 h. In our calculation, 1331 ($11\times11\times11$) air parcels were initially assigned to a small cubic space with range of $\pm0.5°$ in longitude and in latitude at a selected level over Linan.

The trajectory on 15 March shows that the O_3-rich air mass originated and had spent 3 d in its early journey in the boundary layer of south China region and more specifically close to the Pearl River Delta (PRD) region. This is why there was high relative humidity accompanying the high O_3 air masses, as the air in the subtropical south China is high in water content. After that, it traveled in a general southwesterly direction to LinAn. The PRD contains the most industrialized and urbanized cities in south China. There are heavy burdens of pollutant emission from the major cities of the

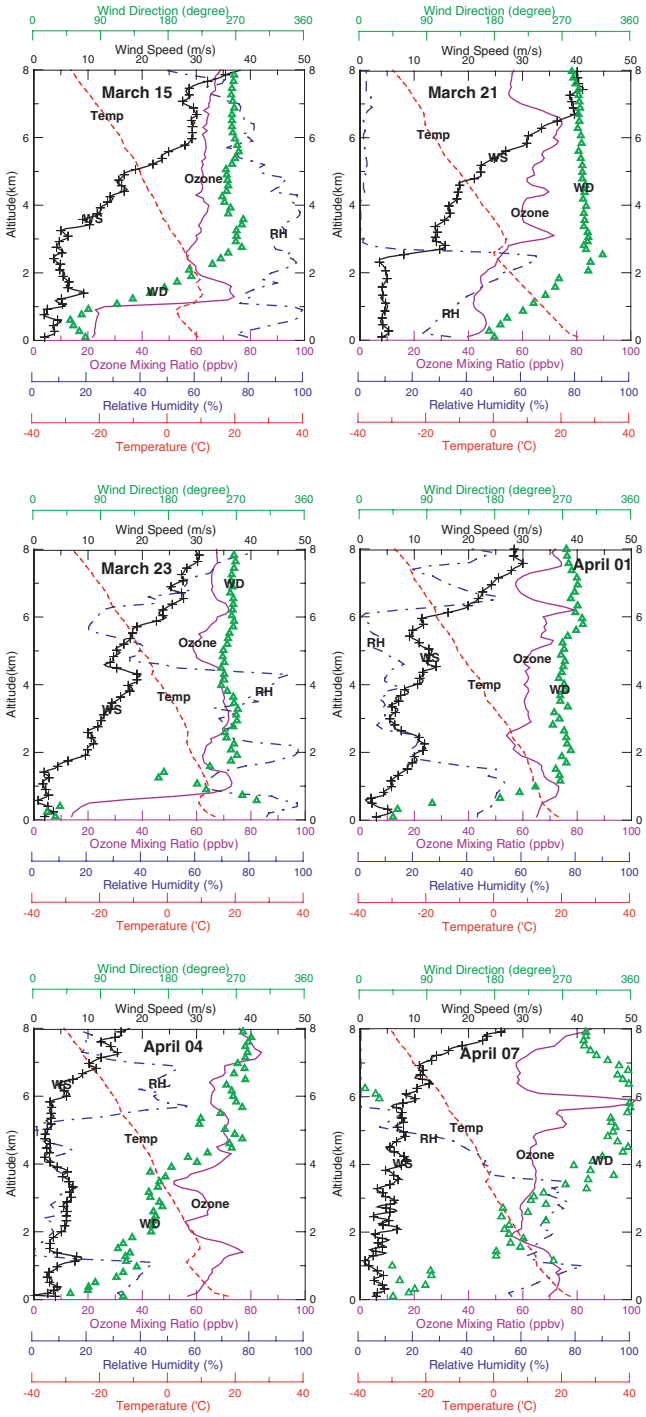

Fig. 7. The vertical profiles of ozone (ppbv), relative humidity (%), wind speed (m s^{-1}), wind direction (degree), and temperature (^{o}C) below 8 km on 21, 15 and 23 March and April 1, 4 and 7.

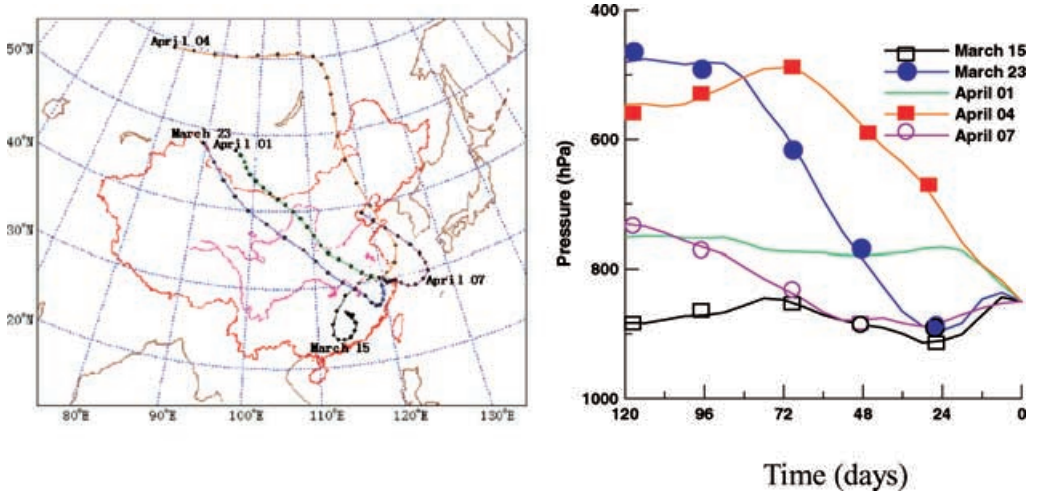

Fig. 8. The 5-d backward air trajectory reaching LinAn at 850 hPa (∼1.4 km) on 21 and 23 March and 1, 4 and 7 April. The right panel is the vertical motion of the trajectory.

region, such as Guangzhou, Macau and Nahai (Wang et al., 2002) and Hong Kong (Fu et al., 1997). Chan and Chan (2000) and Chan et al. (2002b) measured high levels of CO, O_3 and hydrocarbons in air masses passing through the region. Thus, it is possible that the high O_3 observed over LinAn on 15 March was due to the transport of O_3 along the PRD region pollution plume. On 23 March the trajectory shows that the O_3-rich air mass originated from northwest China and traveled to the south China region close to the coast before curving in a northerly direction one day before reaching LinAn. The air mass experienced substantial descending motions from the middle altitude at 500 hPa in its early journey to the boundary layer 1.5 d before reaching LinAn. This is possibly why the O_3-rich air had fairly high relative humidity. There are also pollutant emissions from industrial and urban activities along the subtropical south China coast. It is thus also possible that the air mass had picked up anthropogenic O_3 from the region.

The trajectory on 1 April shows that the air mass originated from northwest China and traveled in a northwest direction to LinAn. On 4 April the air mass originated from a high latitude of northwest Asia and traveled in a northwest direction over northeast China, the Yellow Sea and the East Sea in northeast China before reaching LinAn. The air mass descended substantially from the middle troposphere and remained for relatively less time (1 d) close to the boundary layer. The air mass on 7 April traced back to the northeast China coast in 5 d and traveled in a northwest direction close to the sea surface of the East Sea before turning in an easterly direction 2 d before reaching LinAn. The relative humidity of this air mass is thus higher (80%) than that of the former two air masses (∼50%). Note that the O_3-rich air masses on 4 and 7 April passed through the northeast China coast and the Yangzhi River Delta (YZRD) region of east China. The northeast China coast and the YZRD region contain the most industrialized and urbanized zones of east and northeast China. There are substantial pollutant emissions in these areas (Wang et al., 2001). Thus it is possible that the air masses had picked up the pollutants and O_3 during their journey to LinAn. The O_3 is believed to be anthropogenic in nature, formed through photochemical production from human pollution.

Most air masses reaching LinAn passed over polluted regions of inland China as demonstrated by trajectories. However, not all these air masses contained elevated O_3 levels. This is because photochemical O_3 formation and accumulation also depend on meteorological conditions. Our O_3 launches were performed in the early to middle spring of 2001. The temperature profiles from radiosondes revealed that the weather was still cold most of time within the period. Such weather conditions were not favorable for O_3 formation. This is possibly why only few O_3 episodes were observed even though most air masses had passed over the polluted regions.

4. Conclusion

In this paper we reported and analyzed the tropospheric O_3 measured on the east China coast over LinAn in spring 2001. The PV and back air trajectory were used to distinguish natural O_3 from the transported air from the stratosphere and to trace the source region of anthropogenic O_3 in the boundary layer. The measurement showed that extremely high O_3 mixing ratios sometimes penetrated deep into the 8.5–16 km ASL region as a result of lowering of the tropopause across the East Asia strong STJ stream. Also, high O_3 occurred in the upper and middle troposphere following the extreme O_3 regimes and caused an overall high O_3 mixing ratio in these regions. The occurrence of the high O_3 tongues followed the propagation of dry air with low relative humidity and high potential vorticity, suggesting that the O_3 is of stratospheric origin rather than anthropogenic O_3 resulting from O_3 production from its precursor emission and transport. The exchange of stratospheric O_3 in the upper and middle troposphere was linked to the stratospheric folding process associated with the subtropical east Asia jet. High O_3 episodes were observed in the lower troposphere and especially in the boundary layer. Trajectory analysis suggested that the O_3-rich air masses in the boundary layer had passed through the source regions such as the PRD region of south China, the northeast China coast and the YZRD region of east China. These suggested that the O_3 is of anthropogenic origin resulting from photochemical O_3 formation from the pollutants emitted from industrial and urban activities in these regions. Our analysis thus revealed that over the east China coast at LinAn, stratospheric O_3 is still the predominant source of O_3 in the middle and upper troposphere, while anthropogenic pollution caused high O_3 pollution episodes in the boundary layer in spring 2001.

5. Acknowledgments

This study is supported by a grant from the Research Grant Council of Hong Kong (PolyU 5061/99E), an institutional research grant of The Hong Kong Polytechnic University (G-YW 58) and partly from a grant from the National Natural Science Foundation of China (Grant No. 49975026).

REFERENCES

Akimoto, H., Mukai, H., Nishikawa, M., Murano, K., Hatakeyama, S. et al. 1996. Long-range transport of ozone in the East Asian Pacific Rim Region. *J. Geophys. Res.* **101**, 1999–2010.

Appenzeller, C. and Davies, H. C. 1992. Structure of stratospheric intrusions into the troposphere. *Nature* **358**, 570–572.

Austin, J. F. and Midgley, R. P. 1994. The climatology of the jet stream and stratospheric intrusions of ozone over Japan. *Atmos. Environ.* **28**, 39–52.

Carmichael, G. R., Uno, I., Phadnis, M. J., Zhang, Y. and Sunwoo, Y. 1998. Tropospheric ozone production and transport in the springtime east Asia. *J. Geophy. Res*. **103**, 10 649–10 671.

Chan, C. Y. and Chan, L. Y. 2000, The effect of meteorology and air pollutant transport on ozone episodes at a subtropical coastal Asian city, Hong Kong. *J. Geophys. Res.* **105**, 20 707–20 719.

Chan, C. Y., Chan, L. Y., Harris, J. M., Oltmans, S. J., Blake, D. R. et al. 2002a. Characteristics of biomass burning emission sources, transport and chemical speciation of enhanced springtime ozone profile over the troposphere of the Hong Kong area. *J. Geophys. Res.* **108** (D1), DOI: 10.1029/2001JD001555.

Chan, C. Y., Chan, L. Y., Lam, K. S., Li, Y. S., Harris, J. M. et al. 2002b. The effect of Asian pollutant transport and photochemistry on the CO variability and ozone in subtropical coastal South China, Hong Kong. *J. Geophys. Res.* **107** (D), DOI: 10.1029/2002JD002131.

Chan, C. Y., Chan, L. Y., Zheng, Y. G., Harris, J. M., Oltmans, S. J. et al. 2001. Effects of 1997 Indonesian forest fires on tropospheric ozone enhancement, radiative, and temperature change over the Hong Kong region. *J. Geophys. Res.* **106**, 14 875–14 885.

Chan, L. Y., Chan, C. Y. and Qin, Y. 1998a. Surface ozone pattern in Hong Kong. *J. Appl. Meteorol.* **37**, 2003–2016.

Chan, L. Y., Liu, H. Y., Lam, K. S., Wang, T., Oltmans, S. J. et al., 1998b. Analysis of the seasonal behavior of tropospheric ozone at Hong Kong. *Atmos. Environ*. **32**, 159–168.

Chan, L. Y., Chan, C. Y., Liu, H. Y., Christopher, S., Oltmans, S. J. et al. 2000. A case study on the biomass burning in Southeast Asia and enhancement of tropospheric ozone over Hong Kong. *Geophys. Res. Lett.* **27**, 1479–1482.

Ding, Y. 1994. *Monsoons over China*. Kluwer Academic Publishers, The Netherlands.

Fishman, J. and Brackett, V. G. 1997. The climatological distribution of tropospheric ozone derived from satellite measurements using version 7 Total Ozone Mapping Spectrometer and Stratospheric Aerosol and Gas Experiment data sets. *J. Geophys. Res.* **102**, 19 275–19 278.

Fu, J. M., Sheng, G. Y., Chen, Y., Wang, X. M., Ming, Y. S. et al. 1997. Preliminary study of organic pollutants in air of Guangzhou, Macao and Hong Kong, *ACS Sym Ser.*

671: Molecular Markers in Environmental Geochemistry, 164–175.

Harris, J. M., Oltmans, S. J., Diugokencky, E. J., Novelli, P. C., Johnson, B. J. et al. 1998. An investigation into the source of the springtime tropospheric ozone maximum at Mauna Loa Observatory. *Geophys. Res. Lett*. **25**, 11 189–11 898.

Jacob, D. J., Logan, J. A. and Mupti, P. P. 1999. Effects of rising Asian emissions on surface ozone in the United States. *Geophys. Res. Lett*. **26**, 2175–2178.

Jaffe, D., Anderson, T., Covert, D., Kotcheriruther, R., Trost, B. et al. 1999. Transport of Asian air pollution to North America. *Geophys. Res. Lett*. **26**, 711–714.

Kajii, Y., Someno, K., Tanimoto, H., Hirokawa, J., Akimoto, H. et al. 1998. Evidence for the seasonal variation of photochemical activity of tropospheric ozone, Continuous observation of ozone and CO at Happo, Japan. *Geophysics. Res. Lett*. **25**, 3505–3508.

Komhyr, W. D., Barnes, R. A., Brothers, G. B., Lathrop, J. A. and Opperman, D. P. 1995. Electrochemical concentration cell ozonesonde performance evaluation during STOIC 1989. *J. Geophys. Res.* **100**, 9231–9244.

Langford, A. O. 1999. Stratosphere–troposphere exchange at the subtropical jet contribution to the tropospheric ozone budget at midlatitudes. *Geophys. Res. Lett*. **26**, 2449–2452.

Logan, J. A. 1985. Tropospheric ozone: seasonal behavior, trends, and anthropogenic influence. *J. Geophys. Res.* **90**, 463–482.

Luo, C., St. John, J. C., Zhou, X. J., Lam, K. S., Wang, T. et al. 2000. A nonurban ozone air pollution episode over eastern China: Observation and model simulations. *J. Geophys. Res.* **105**, 1889–1908.

Ma, J., Liu, H. and Hauglustaine, D. 2002. Summertime tropospheric ozone over China simulated with a regional chemical transport model 1. Model description. *J. Geophys. Res.* **107** (D22), 4660, DOI: 10.1029/2001JD001354.

Miyazaki, Y., Kita, K., Kondo, Y., Koike, M., Ko, M. et al. 2003. Springtime photochemical ozone production observed in the upper troposphere over east Asia. *J. Geophys. Res.* **108** (D3), 8398, DOI: 10.1029/2001JD000811.

Monk, P. S. 2001. A review of the observations and origins of the spring ozone maximum. *Atmos. Environ.* **34**, 3545–3561.

Muramatsu, H., Sasaki, T., Hirota, M. and Makino, Y. 1984. An Aircraft observation of an intrusion process of stratospheric ozone into the troposphere. *Meteorol. Geophys.* **35**, 1–10.

Murao, N., Ohta, S., Noritaka, F. and Mizoguchi, I. 1990. The cause of elevated ozone concentrations in Sapporo. *Atmos. Environ*. **24**, 1501–1507.

Murayama, S., Yamazaki, K., Nakazawa, T. and Aoki, S. 1998. Interpretation of high mixing ratios of O_3 observed in the upper troposphere over Syowa Station, Antarctica using a trajectory analysis. *Geophys. Res. Lett*. **25**, 1177–1180.

Newell, R. E., Browell, E. V., Davis, D. D. and Liu, S. C. 1997. Western Pacific tropospheric ozone and potential vorticity: Implications for Asian pollution. *Geophys. Res. Lett*. **24**, 2733–2736.

Oltmans, S. J. and Levy, H. II. 1992. Seasonal cycle of surface ozone over the western north Atlantic. *Nature* **358**, 392–394.

Pocharnart, P., Hirokawa, J., Kajii, Y., Akimoto, H. and Nakao, M. 1999. The influence of regional scale anthropogenic activity in the Northeast Asia on seasonal variations of surface ozone and its precursors observed at Oki, Japan. *J. Geophys. Res.* **104**, 3621–3631.

Sunwoo, Y., Carmichael, G. R. and Ueda, H. 1994. Characteristics of background surface ozone in Japan. *Atmos. Environ*. **28**, 25–37.

Tang, X., Li, J. and Chen, D. 1995. Summertime photochemical pollution in Beijing. *Pure Appl. Chem.* **67**, 1485–1495.

Tsutsumi, Y. and Makino, Y. 1995. Vertical distribution of the tropospheric ozone over Japan: the origin of the ozone peaks. *J. Meteorol. Soc. Jpn.* **73**, 1041–1058.

Wakamatsu, S., Uno, I., Ueda, H., Uehara, K. and Tateishi, H. 1989. Observational study of stratospheric ozone intrusions into the lower troposphere. *Atmos. Environ*. **23**, 1815–1826.

Wang, T., Cheung, V. T. F., Anson, M. and Li, Y. S. 2001. Ozone and related gaseous pollutants in the boundary layer of eastern China: Overview of the recent measurements at a rural site. *Geophys. Res. Lett*. **28**, 2373–2367.

Wang, X. M., Sheng, G. Y., Fu, G. M., Chan, C. Y., Lee, S. C. et al. 2002. Urban ground levels of BTEX at three cities in the Pearl River Delta region. *Atmos. Environ.* **36**, 5141–5148.

Yamazaki, K., Okada, H. and Iwasaka, Y. 1989. Where do aerosol particles in the Antarctic upper troposphere come from? (a case study in January 1983). *J. Meteorol. Soc. Jpn.* **67**, 889–906.

Yienger, J. J., Galante, M., Holloway, T. A., Phadnis, M. J., Guttikunda, S. K. et al. 2000. The episodic nature of air pollution transport from Asia to North America. *J. Geophys. Res.* **105**, 26 931–26 945.

Zhang, M., Uno, I., Sugata, S., Wang, Z., Byun, D. and Akimoto, H. 2002. Numerical study of boundary layer ozone transport and photochemical production in east Asia in the wintertime. *Geophys. Res. Lett.* **29**, 40-1–40-4.